University of Wollongong

Research Online

2018

Sintering of Iron Ores in a Millipot in Comparison with Tablet Testing and Industrial Process

Huibin Li
University of Wollongong, huibin@uow.edu.au

Di Zhou
BlueScope Steel Limited

David J. Pinson
University of Wollongong, DavidJ.Pinson@bluescopesteel.com

Paul Zulli
University of Wollongong, paulz@uow.edu.au

Liming Lu
University of Wollongong, Liming.Lu@csiro.au

See next page for additional authors

Sintering of Iron Ores in a Millipot in Comparison with Tablet Testing and Industrial Process

Abstract

To explore the feasibility of small-scale sintering pot testing, a 'millipot' facility (diameter of 53 mm and height of 400 mm) was established and used to examine the sintering performance of iron ores and other non-traditional ferrous materials. The sintering performance of a millipot was examined across a range of different operational conditions (coke rate and suction pressure) and compared with an industrial sinter strand operation. Tablet tests were also performed to assist in the design of the millipot experiments and identify conditions for achieving mineral composition similar to the industrial sinter. For the millipot experiments, the materials used need to be compacted to increase the bulk density, and a higher coke rate is required to compensate the high heat loss caused by wall effects. A higher suction pressure is also necessary to maintain an oxidizing atmosphere in the sinter bed. As expected, it was not possible to eliminate the wall effect, which resulted in more primary hematite at edges of the sintered column. However, the sintered material from the center of column simulates industrial sinter reasonably well. As such, millipot provides a practical way to evaluate the sintering process and material performance at laboratory scale, helping to bridge the gap between tablet sintering and large scale pot sintering, or full scale plant trial. The results of millipot testing can be used for designing larger scale experiments or commercial sintering trials.

Disciplines

Engineering | Science and Technology Studies

Publication Details

Authors

Huibin Li, Di Zhou, David J. Pinson, Paul Zulli, Liming Lu, Raymond Longbottom, Sheng Chew, Brian J. Monaghan, and Guangqing Zhang

Sintering of Iron Ores in a Millipot in Comparison with Tablet Testing and Industrial Process

Huibin LI[1], Di ZHOU[2], David J. PINSON[1,2], Paul ZULLI[1], Liming LU[3], Ray J. LONGBOTTOM[1], Sheng J. CHEW[1,2], Brian J. MONAGHAN[1], Guangqing ZHANG[1*]

1). ARC Research Hub for Australian Steel Manufacturing, School of Mechanical, Materials Mechatronics and Biomedical Engineering, University of Wollongong, Wollongong, NSW 2500.

2). BlueScope Steel, Port Kembla, NSW 2505.

3). CSIRO Queensland Centre for Advanced Technologies, Brisbane, QLD 4069.

*Corresponding author: Guangqing Zhang, Email: gzhang@uow.edu.au

10 **Abstract**

11 To explore the feasibility of small-scale sintering pot testing, a 'millipot' facility (diameter of

12 53 mm and height of 400 mm) was established and used to examine the sintering

13 performance of iron ores and other non-traditional ferrous materials. The sintering

14 performance of a millipot was examined across a range of different operational conditions

15 (coke rate and suction pressure) and compared with an industrial sinter strand operation.

16 Tablet tests were also performed to assist in the design of the millipot experiments and

17 identify conditions for achieving mineral composition similar to the industrial sinter. For the

18 millipot experiments, the materials used need to be compacted to increase the bulk density,

19 and a higher coke rate is required to compensate the high heat loss caused by wall effects. A

20 higher suction pressure is also necessary to maintain an oxidizing atmosphere in the sinter

21 bed. As expected, it was not possible to eliminate the wall effect, which resulted in more

22 primary hematite at edges of the sintered column. However, the sintered material from the

23 centre of column simulates industrial sinter reasonably well. As such, millipot provides a

24 practical way to evaluate the sintering process and material performance at laboratory scale,

25 helping to bridge the gap between tablet sintering and large scale pot sintering, or full scale

26 plant trial. The results of millipot testing can be used for designing larger scale experiments

27 or commercial sintering trials.

28 **KEY WORDS:** sintering of iron ores, tablet testing, millipot, industrial sinter, mineral

29 composition of sinter, microstructure of sinter

1. Introduction

At present, sinter is the major ferrous burden material used in the blast furnace (BF) for the production of hot metal, which accounts for about 70% of the world's steel production annually. [1, 2] However, with ever changing ore costs and specifications, steelmakers are increasingly motivated to use iron ore resources with a wider range of grades and mineral types previously considered unsuitable or uneconomical for sintering, as well as other iron-bearing materials such as plant by-products. This means that new issues requiring further investigation and understanding continue to arise, including the sintering of ore types with a) overall higher gangue content, b) elements that cause problems in the steel manufacturing operations, and c) distinctive sintering performance compared with traditional hematite-rich iron ores.

Laboratory-based investigation of the sintering performance and the behaviour of the gangue components during sintering is an important step towards the successful utilization of these resources in steelmaking. In terms of laboratory-based sintering investigations, there are two generally accepted experimental scales utilized prior to industrial-scale trials being undertaken, *viz.* bench-scale tablet (compact) testing [3-7], and pilot-scale pot testing [2, 8-12]. The former has the advantages of flexibility and more precise control of sintering conditions, but the effects of particle size and heterogeneity of the blend are neglected. The latter, which is carried out in pots with diameters between 150~500 mm, simulates the industrial sintering process and conditions, producing product sinter suitable for standard testing regimes, but is time consuming and labor-intensive. It is therefore desirable to develop a smaller scale pot testing facility, a "millipot", which avoids the above disadvantages of a large sinter pot but still provides industrially relevant information.

Neither bench- nor pilot-scale can fully simulate the industrial sintering process. In order to obtain better simulation performance, especially in the formation of mineral phases during

3

55　high temperature sintering, the selection of the operating parameters in bench- and pilot-scale

56　testing is crucial. In previous tablet testing investigations, an oxygen partial pressure of 0.5

57　kPa and 4 minutes sintering at target temperatures were used to simulate the local atmosphere

58　in the sintering hot zone. [6, 7] In sinter pot testing, parameters, such as bulk density of sinter

59　bed, suction pressures during ignition and sintering, and ignition time were considered. [2,

60　12, 13] In this work, the parameters of millipot runs were adjusted on the basis of the

61　previous investigations to get better sintering performance. The mineral composition of the

62　sinter samples from the millipot was investigated at different coke rates and compared with

63　an industrial sinter obtained from the same green feed. Corresponding sintering conditions to

64　generate similar mineral phases in tablet testing were also explored. The objectives were to

65　develop a fundamental understanding of the microtextural characteristics at three scales

66　(tablet, millipot and industrial) and to demonstrate the suitability and application of the

67　millipot set-up to simulation of the industrial sintering process.

68　**2.　Experimental**

69　**2.1　Sintering Feed Materials**

70　As one of the objectives of the present work was to closely simulate industrial sintering

71　conditions, green feed from the exit of the granulation drum at BlueScope's Port Kembla

72　Sinter Plant was used as the base feed for the millipot experiments. The components of the

73　base green feed were (wet-wt%-green feed basis at a total free moisture content of 6%):

74　　• Iron ores (Ores 1 to 5): 45.7, 1.82, 1.51, 1.69 and 8.31 wt%, respectively.

75　　• Manganese ore, ferrous recycles, metallic recycles and returned fines: 0.34, 4.70, 3.23

76　　　and 15.65 wt%, respectively.

77　　• Limestone and dolomite: 10.62 and 2.28 wt%, respectively.

78   • Coke: 4.17 wt%.

79   The mixed green feed was sampled and then stored in sealed plastic bags to prevent loss of

80   moisture. To determine its particle size distribution, a sub-sample was dried and sieved,

81   resulting in a distribution (wt%) of: +0-2mm 37%, +2-4mm 29%, +4-6.3mm 19%, +6.3-8mm

82   6%, +8-10mm 4% and +10mm 5%.

83   Due to the small diameter of the millipot, large particles have a disproportionate effect on the

84   local sintering conditions. [11] To mitigate this, the feed was sieved with the +6.3 mm

85   fraction being jaw crushed and recombined before manual regranulation in a laboratory drum

86   to ensure the final green feed had a top size less than 6.3 mm. The indicative green feed

87   composition was (wt% dry basis, including all components in the blend): total Fe 47.8 (1.76

88   FeO), SiO_2 5.56, Al_2O_3 1.51, CaO 8.71, MgO 1.01 and carbon 3.99 yielding a basicity

89   (CaO/SiO_2 weight ratio) of 1.57.

90   The coke rate was defined as follows:

91                $$\text{Coke rate (CR)} = \frac{m(\text{coke})}{m(\text{green feed})} \times 100\% \qquad (1)$$

92   where m(coke) denotes the mass of coke and m(green feed) the mass of green feed including

93   coke, both on a dry basis.

94   For tablet experiments, an equivalent blend comprising the ore and flux components (coke

95   and recycles were not included) was sourced from the plant raw material stockpiles, with

96   each raw material component ground to < 200 µm. These materials were then mixed in the

97   proportion corresponding to that of the industrial sinter plant and mixed thoroughly to ensure

98   homogeneity.

2.2 Sintering Equipment

100 Figure 1(a) shows a schematic of the millipot: it consists of an insulated sinter tube (pot), air

101 suction and waste gas treatment components, and a process monitoring and control system.

102 The sintering tube is a stainless-steel column (53 mm internal diameter, 490 mm high)

103 surrounded by 50 mm of thermal insulation material. Six ports on the side of the column

104 allow for insertion of thermocouples to monitor the sintering temperature, or connection with

105 a differential pressure transducer for pressure drop measurement. Two extra ports are

106 available at the bottom extended section (T7) for the measurement of off-gas temperature and

107 the pressure drop across the sinter bed. The sintering process is initiated using an LPG burner

108 located at the top of the millipot. The air suction system includes a water ring vacuum pump

109 and a buffer container or windbox to stabilize the system suction pressure. The windbox is

110 half filled with water so that the flue gas generated during sintering can be cooled and

111 cleaned before passing through the suction pump. The suction pressure can be controlled

112 using a bypass valve on the windbox providing additional dilution air, *i.e.* without flowing

113 through the sinter pot.

114 The process monitoring system measures the sintering temperature and pressure drop within

115 the sinter pot. The temperatures at different locations of the sinter pot are monitored using

116 bare Type K thermocouples connected to a Thermocouple C Series Module (Model NI 9212,

117 National Instruments). Bare thermocouples were used to increase the sensitivity and accuracy

118 of the measurement. The suction pressure is monitored using a differential pressure

119 transducer (26PC series, Honeywell, supplied by RS Australia) with one side connected to

120 port P and the other to ambient. All of the temperature and pressure data are logged using a

121 computer with LabVIEW software (version 2013.0.1, National Instruments).
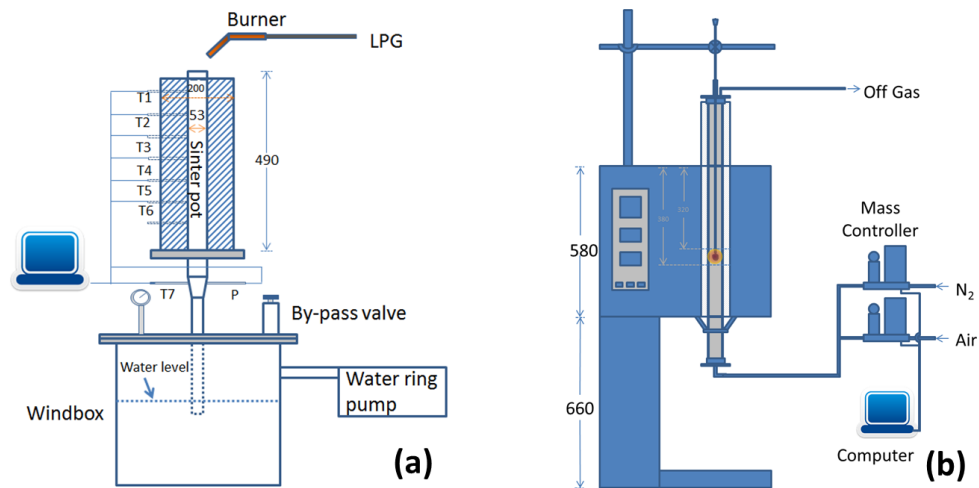
Figure 1. Schematics of laboratory sintering set-ups: (a) Millipot; (b) vertical electrical furnace.

The tablet sintering experiments were carried out using a vertical electric heating tube furnace as presented in Figure 1(b). Tablets were loaded into a steel wire basket and located in the furnace hot zone. The oxygen partial pressure was adjusted by mixing air and nitrogen, with flow rates controlled via mass flow controllers. The parameters of individual experiments are covered in the Results and Discussion section.

2.3   Sintering Procedures

For the millipot testing, the green feed was added to the stainless steel column in approximately 120g aliquots and compacted with a rod after each aliquot was added. Thermocouples were placed in the corresponding port as filling approached the level of each port. Sintering was initiated by adjusting suction pressure to 5.3 kPa and then placing the burner over the top of the bed for 90 s. The burner was then removed and the suction pressure increased to 10.6 kPa, matching the pressure gradient used by Lu. [2, 13] After the flame front had passed through the bed, suction was continued until the flue-gas temperature cooled to 80 °C, following which the pump was turned off and the sinter pot unloaded. Sintered

139   lump products excluding the wall area were collected for analysis. A more detailed procedure

140   for the millipot operation is reported elsewhere. [12]

141   Flame front speed (FFS) is an important operational parameter for sintering. In this

142   investigation, the FFS is defined as follows:

143   $$\text{FFS} = \frac{Bed\ height}{Sintering\ time} \qquad (2)$$

144   It is calculated using the distance between ports 1 and 6 (bed height) divided by the time

145   difference at which the peak temperatures were reached at the two ports (sintering time).

146   For the tablet experiments, cylindrical tablets of 6 mm diameter and ~5 mm height were

147   prepared. An equivalent tablet blend was prepared from individual ores and fluxes (without

148   coke and recycles) in the normalised proportions present in the plant green feed. The tablet

149   blend was ground in a ring mill to less than 200 µm and pressed at 48.8 MPa to form each

150   tablet. The tablets were loaded into the reaction basket and placed at the top (cold) end of the

151   furnace tube. The furnace was preheated to the desired temperature and flushed with the gas

152   mixture (P_{O_2} = 0.5 kPa) for at least 15 minutes; the basket was lowered to the hot zone and the

153   tablet sintered for 4 minutes with gas flow of 1 NL/min (linear speed: 0.45 m/min). [6]

154   Adopting the methodology of Wang et al. [7], two cooling procedures were employed: a)

155   directly lifting the basket to the cold end of the furnace tube and simultaneously switching the

156   sintering gas atmosphere to ambient air; b) soaking at the sintering temperature or 1250 °C,

157   whichever was lower, in air of 6 NL/min for 3 minutes, then lifting the basket to the top end

158   of the furnace tube. All the temperatures were pre-calibrated by lowering a type R

159   thermocouple into the empty hot zone of the furnace with the same gas flow.

160   The overall oxygen partial pressure in the exhaust gas of a sinter strand is high. However, due

161   to the non-uniform gas flow, , and the progression of the flame front, the oxygen partial

162   pressure in a sinter bed is dynamic and non-uniform over a large range (0-21%). In a local

8

163   area where the gas flow is weak and oxygen is consumed by the combustion of coke, the

164   oxygen partial pressure can be very low. In previous investigations it was shown that 0.5%

165   O_2 partial pressure was a representative value for the formation of mineral phases during high

166   temperature sintering, and was determined for tablet sintering conditions to produce similar

167   overall microstructures. [6, 7] This O_2 partial pressure value was therefore used in this

168   investigation in assessing mineral composition effect in tablet sintering.

2.4   Characterization Methods

170   The sintered tablets and lump sinter samples were mounted in epoxy resin in preparation for

171   optical and SEM-EDS analysis. After curing, the surface was ground and polished to a 1 μm

172   finish for optical microscopic observation (Leica DM6000 Optical Microscope). The polished

173   sample was then platinum coated and analyzed by scanning electron microscopy (JEOL JSM

174   – 6490LV) operated at 15 kV.

175   The mineral phase compositions of the industrial sinter samples were determined by point

176   counting (Olympus Vannox optical microscope) and the millipot samples by image analysis.

177   In both cases, the samples were crushed to less than 1.7 mm, and then 32 g of representative

178   samples were mounted in epoxy resin. After curing, the cylindrical samples were cut along

179   the axial direction and polished to a 1 μm finish. Optical images for image analysis were

180   taken by Leica DM6000 Optical Microscope and analyzed by Leica application Suite V4.0.

3.   Results and Discussion

3.1   Industrial Sintering Conditions and Sinter Properties

183   Sinter quality metrics such as reducibility and mechanical strength affect BF productivity – in

184   turn, sinter quality is governed by its microstructure. Sinter microstructure requires

185   characterization in terms of chemical composition, mineralogy, and morphology of the

186   presenting phases.

187   Figure 2 shows optical images of an industrial sinter sample of the same blend. During

188   production of that sinter, the bulk density of green feed was 1770 kg/m^3 and FFS was 13.6

189   mm/minute. Silico-ferrites of calcium and aluminum, SFCA and SFCA-I, are typically the

190   major and most desirable bonding phases because of their high reducibility and good

191   mechanical strength. [14-19] Moreover, the SFCA phases are considered the most important

192   phases for producing high quality sinter at low temperatures and high productivity. [20-23]

193   Secondary hematite and magnetite are the second group of major constituents in the bonding

194   phases which are formed in more oxidizing or reducing atmospheres, respectively, and

195   crystallized from the melt. Additionally, some relict regions (quartz and primary hematite

196   derived from goethite ore) retain their original contours and show a reaction halo with the

197   surrounding melt, Figure 2e.
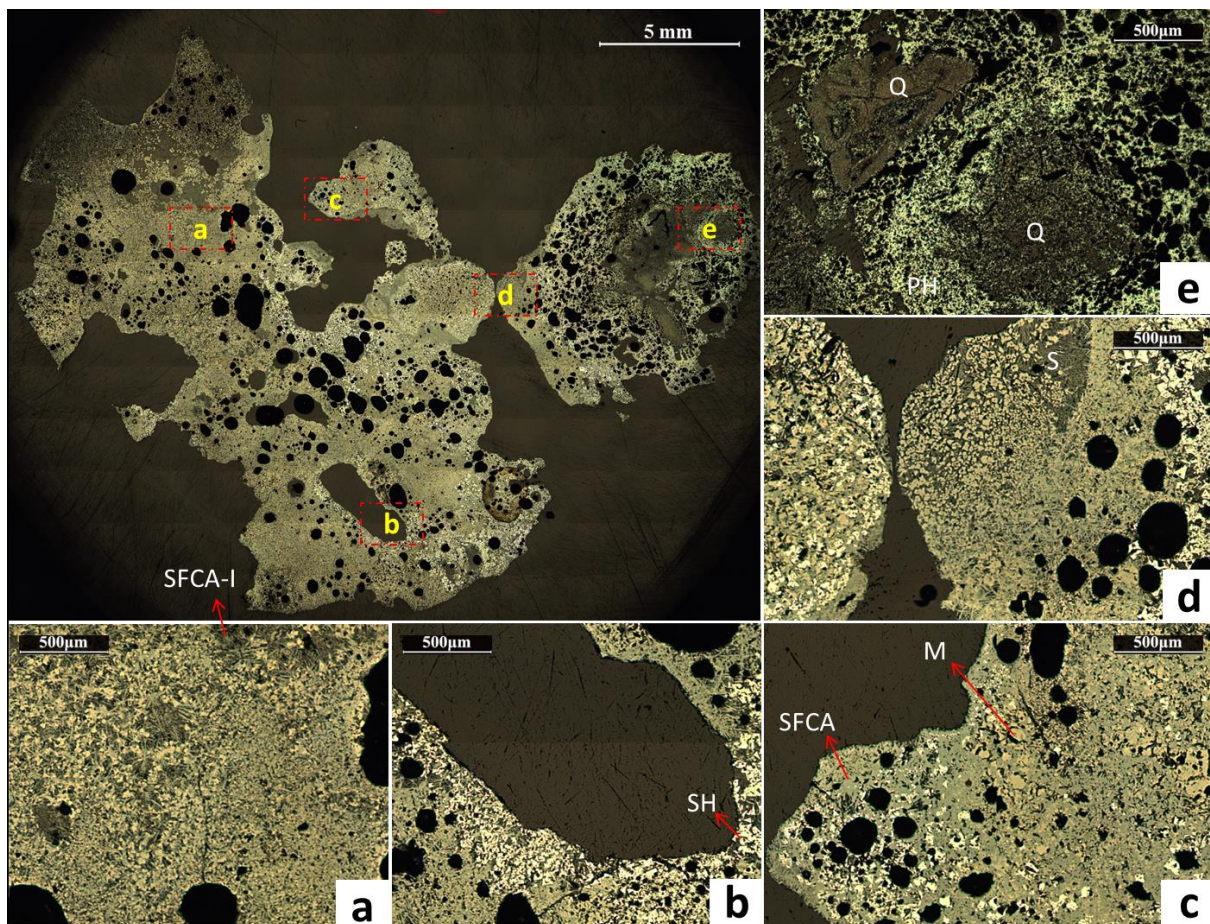
198

199   Figure 2. Optical images of industrial sinter. Q: quartz; PH: primary hematite; SH: secondary

200   hematite; M: magnetite; S: silicate; SFCA: platy shape of silico-ferrite of calcium and

201   aluminum; SFCA-I: acicular shape of silico-ferrite of calcium and aluminum.

202   Figure 2 shows that individual particles of the industrial sinter sample, and also different

203   regions within those particles have distinctive morphologies and mineral compositions. It is

204   understood that the differences were caused by the changes of the sintering conditions at

205   different locations of the sintering bed due to local non-uniformity of the blend composition,

206   loading density, gas flow, etc., which caused differences in the maximum temperatures reached

207   and oxygen partial pressure at different locations. However, it was the general morphology and,

208   specifically, the overall mineral phase composition of the industrial sinter that was targeted for

209   the millipot sinter product.

210   **3.2   Sintering Performance of Millipot**

211   In this millpot study, the material being sintered was derived directly from sinter plant green

212   feed, with adjustment of coke rate being made to achieve reasonably close correspondence of

213   sintering conditions to those in the full-scale plant. The feed preparation and experimental

214   procedures for the millipot were adjusted by comparison to the sintering performance of the

215   industrial process, as summarized below.

216   An initial set of experiments were carried out to investigate the effect of coke rate and

217   determine an appropriate level for the millipot runs with no initial compaction of the green

218   bed. [12] However, without compaction, the FFS was significantly higher than in the

219   industrial sinter strand, 18~24 cf. ~14 mm/min, and approximately half of the sintered

220   material was in the form of fines (<3.35mm), *i.e.* insufficient melting phase was formed to

221   bond materials together. Furthermore, the bulk density of green feed without compaction was

222   ~1650 kg/m^3, which was lower than an optimum level of ~1800 kg/m^3 [2] - this resulted in a

223   high sinter bed permeability and ultimately high FFS, high heat loss and low melt formation.

224   To increase the density, uniformity and controllability of pot filling, and to decrease the FFS

225   during sintering, a compaction rod with a 50 mm diameter disk (weight = 1327 g) at the base

226   was used. The green feed was loaded into the column in 120 g increments (out of a total

227   charge of 1750 g). After each 120 g increment, the compaction rod was gently placed on the

228   surface, lifted 100 mm and then released. This process was repeated until the column was

229   filled to the top giving an initial bed height of 400 mm. Figure 3 presents the relationship

230   between the loaded weight and the bed height, and corresponding average bulk density at

231   different loading heights. Using the compaction rod, the bulk density of the sinter bed

232   attained ~1880 kg/m^3. There was a slight difference between the bottom and top of the bed

233   and the trend was repeatable.
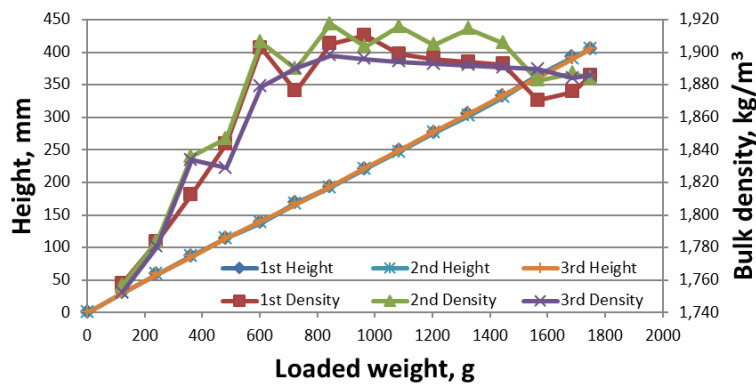
234

235   Figure 3. The changes of the bed height and average bulk density with the loaded weight. The

236   bed height lines overlap.

237   The effect of coke rate on the sintering performance is presented in Table 1. With

238   compaction, the average bulk density ranged between 1870-1880 kg/m^3. The FFS at different

239   coke rates was reasonably consistent, i.e. ~16 mm/minute. Except for the test with a low coke

240   rate of 5.0%, all of the tests were well sintered, with less than 15% of fines smaller than 3.35

241   mm in the whole sinter product.

242   Table 1. Effects of coke rate and suction pressure gradient on the sintering performance of

243   iron ores

Test No.	Coke rate, %	Suction pressure				Bulk density, kg/m^3	FFS, mm/min	Fraction of fines <3.35 mm, %	Temperature profile
		Ignition		Sintering					
		kPa	kPa/m	kPa	kPa/m				
1	5.0	5.3	13.3	10.6	26.5	1876	16.6	20.9	Fig. 4(a)
2	6.0	5.3	13.3	10.6	26.5	1880	15.4	11.6	Fig. 4(b)
3	7.4	5.3	13.3	10.6	26.5	1877	15.3	12.8	Fig. 4(c)
4	8.0	5.3	13.3	10.6	26.5	1872	15.1	10.8	Fig. 4(d)
5	6.0	5.6	14.0	11.5	28.8	1874	16.5	14.3	Fig. 4(e)

244

245   Figure 4 presents the temperature profiles and the change of suction pressure during various

246   sintering tests with different coke rates. It should be noted that these temperature profiles

247   likely better reflect gas, rather than solid, temperatures. Furthermore, the measured peak

248   temperature was affected by different factors such as local solid composition and local

249   porosity surrounding the thermocouple tip. These composition/porosity effects are likely to

250   vary between thermocouple to thermocouple and test to test. As such values are qualitative

251   and should be considered with respect to temperature trends than absolute values. The peak

252   temperature at the column centre was always high, increasing down the pot as sintering

253   progressed, which is consistent with the industrial process and traditional sinter pot. The

254   temperature measurement at the wall shows that thermal conditions were not sufficient to

255   effectively sinter the ores. To achieve a uniform coke particle distribution radially and

256   axially, Coke was mixed with ore and fluxing components in the form of particles to simulate

257   the state in the industrial sinter strand, and fully granulated prior to adding to the millipot.

258 The temperature difference between the centre and the wall is principally a result of heat loss

259 at the wall and not from the non-uniform coke distribution.
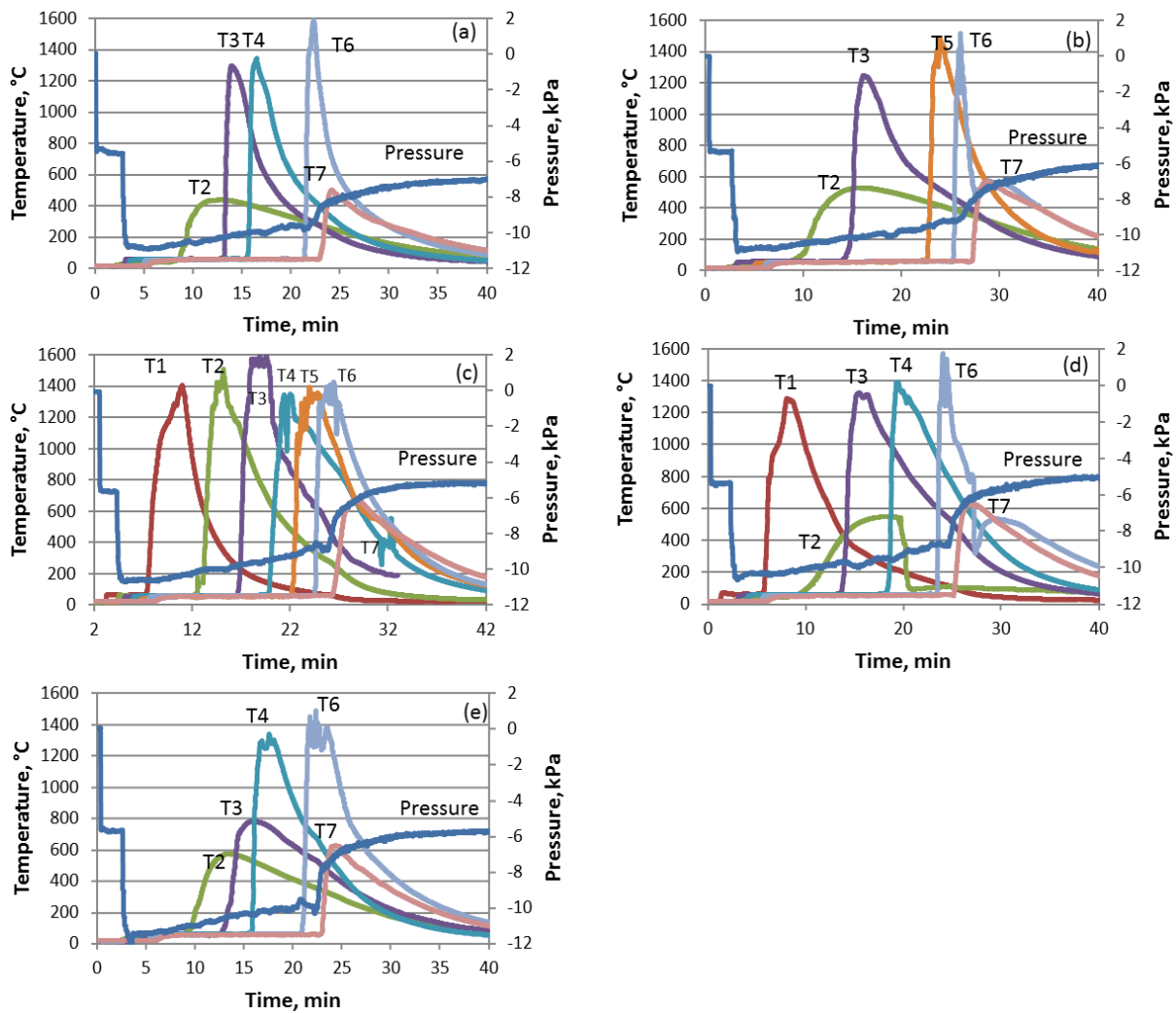
260

261 Figure 4 – Temperature and suction pressure profiles during millipot sintering under different

262 coke rates. (a) Coke rate = 5.0%; T2: wall temperature, and T3, T4, T6: centre temperatures;

263 (b) Coke rate = 6.0%; T2: wall temperature, and T3, T5, T6: centre temperatures; (c) Coke

264 rate = 7.4%; T1 - T6: centre temperatures; (d) Coke rate = 8.0%; T2: wall temperature, and

265 T1, T3, T4, T6: centre temperatures; (e) Coke rate = 6.0%; T2, T3: wall temperatures, and

266 T4, T6: centre temperatures; increased suction pressure. T7: flue gas temperature in all plots.

267 Figure 4 also shows that the suction pressure reduced with the progress of sintering, with a

268 sharp transition after the flame front had passed through the bottom of the sinter bed. The gas

269   flow after the ignition stage was measured to be 64 NL/min, corresponding to a superficial

270   velocity of 2.9 m/s (empty column, at 0 °C and 1 atm). The gradual reduction in the suction

271   pressure before the flame front passed through the whole bed reflects a reduction in flow

272   resistance of the product sinter relative to the feed because of the removal of coke and

273   moisture from the bed, and the coalescence and rearrangement of pores during sintering.

274   Notably, the suction pressure at the end of sintering decreased from 7.2 kPa to 5 kPa (from

275   18.0 kPa/m to 12.5 kPa/m) when the coke rate was increased from 5.0% to 8.0%, which

276   indicates the final permeability was higher as coke rate increased due to enhanced

277   coalescence and higher resultant porosity.

278   Table 1 also includes the result of a sintering test in which the suction pressures at the

279   ignition and sintering stages were both increased in comparison with the reference conditions

280   with coke rate at 6% (test 5). The suction pressure was increased to 5.6 and 11.5 kPa (14.0

281   and 28.8 kPa/m) during ignition and sintering, respectively, in order to increase the oxygen

282   potential. With similar starting bulk density, the increase in suction pressure caused an

283   increase in FFS, with increased fines generation being observed compared to test 2. Despite

284   the negative effect on the extent of sintering, increased suction pressure increased the air flow

285   in the sintering bed, which is beneficial to maintaining a high oxygen partial pressure and the

286   formation of SFCA and hematite.

287   Figure 5 shows the coherent core of the sinter product from testing with 6% coke rate with

288   increased suction pressure (test 5). In general, the core was well sintered except at the edge

289   where some embedded, weakly sintered ore and flux particles can be observed.
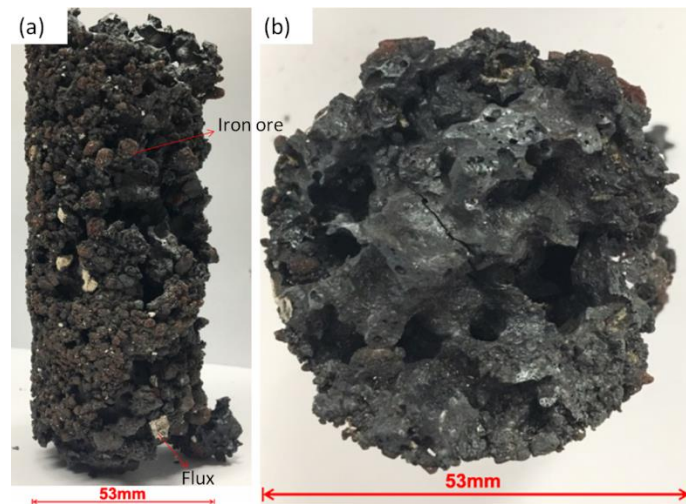
15

290

Figure 5. Photographs of the sinter core from testing with 6% coke rate at increased suction

pressures. (a) Side view; (b) cross-section view.

The sample presented in Figure 5 was mounted in epoxy resin and polished to observe its

microstructure and mineral phases. Figure 6(a) presents a photomicrograph of the sinter

cross-section of the core in Figure 5(a) after grinding and polishing which gives an overview

of sintering performance across the millipot and the influence of wall effects. The most

notable feature is that primary hematite is preferentially distributed near the edge of the cross-

section due to low sintering temperatures near the wall. Figure 6 (d) shows a typical

photomicrograph of the sinter cross-section taken from the centre of the core in Figure 5(a),

and Figures 6 (e) and (f) are the magnified images of the areas marked on Figure 6(d).

Overall, the area in Figure 6(d) was well sintered; the structure contains many round pores,

indicating that the solid was partially melted during sintering. A large amount of magnetite

was observed which was bonded by SFCA, as shown in Figures 6(e) and (f), due to the high

temperature and low oxygen partial pressure atmosphere during the peak temperature period

in the sintering process. In the sinter adjacent to large pores, secondary hematite and SFCA

were observed. After the passage of the flame front, colder air passed through the already

sintered bed on its way to the reaction zone, providing an oxidizing atmosphere during

16

308   cooling. Needle-like larnite in glass was also observed in the lower part of Figure 6(e),

309   reflecting the high peak temperature reached similar to that in the industrial sintering process.

310   Based on the sintering extent as characterized by the morphology and mineral composition, it

311   may be inferred that the temperature distribution was relatively uniform except in the thin

312   layer close to the wall of the sinter column. This phenomenon is likely a result of the

313   relatively fast heat transfer within the metallic millipot wall and the slow heat transfer in the

314   sinter bed.
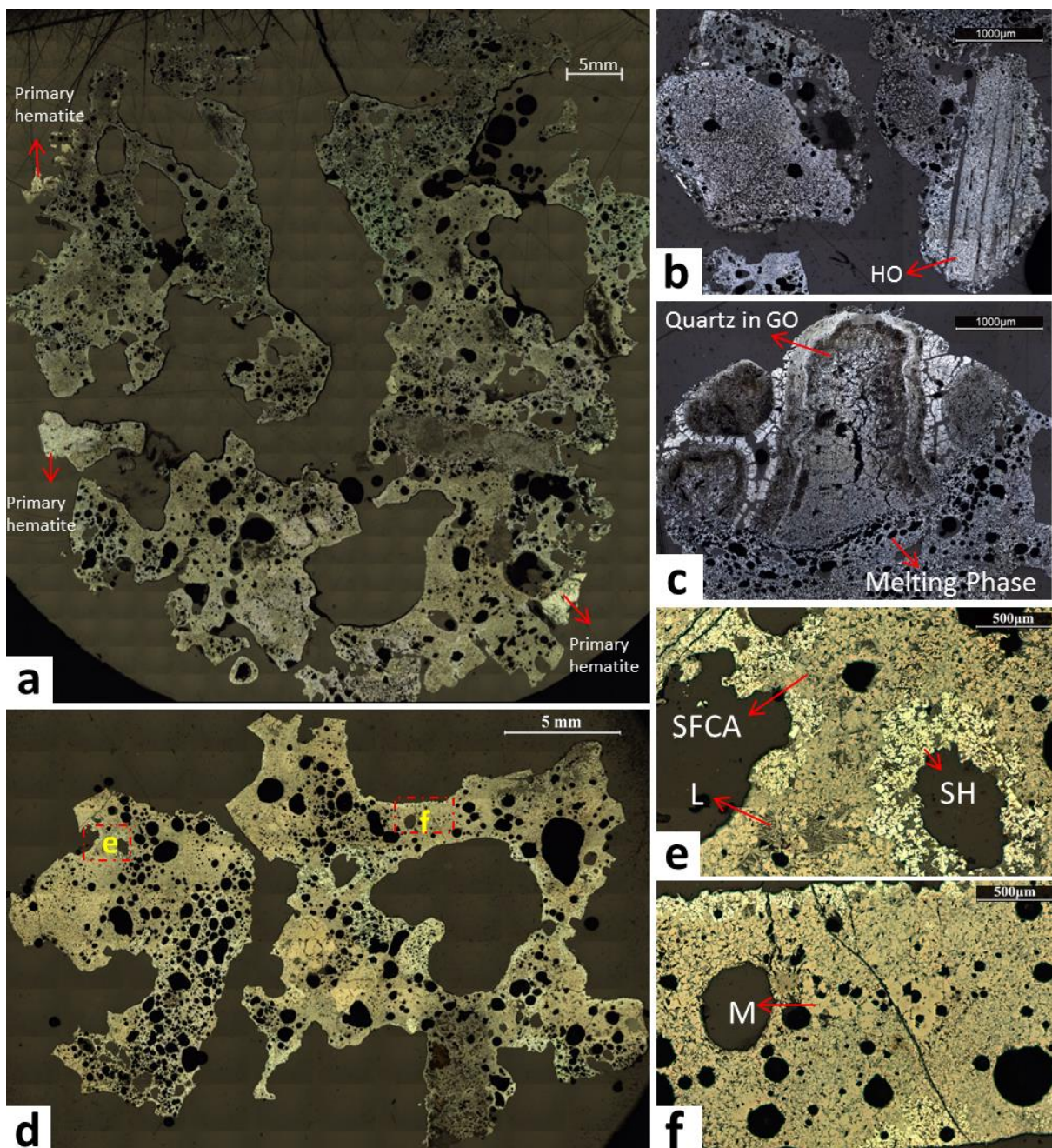
315

316 Figure 6 – Photomicrographs of the sinter core in Figure 5: (a) cross-section of the sinter

317 core; (b), (c) the edge of the core at different section; (d) the centre section of the core; (e), (f)

318 the rectangular areas as marked in (d). GO: goethite ore; HO: hematite ore; L: larnite.

319 Figures 6 (b) and (c) present the microphotographs of typical structures of particles around

320 the edge of the sinter column. Remnant iron ore particles dominate which correspond to those

321 observed macroscopically in Figure 5 (a). Limited assimilation of ore and flux particles

322 occurred at the pot wall where heat losses are high. In Figure 6, some unreacted flux and iron

323 ore particles are present near the edge of the sinter column. Incomplete sintering also took

324 place in some particles: their shapes were retained but pores and secondary hematite were

325 formed during sintering. Classification of the semi-reacted particles in Figures 6 (b) and (c)

326 was inferred based on morphological comparison to unsintered ore samples. Partially melted

327 areas were observed on the edge of the particles, as characterized by porous structure and

328 rounded pores. Due to the significantly lower temperature in the edge zone caused by wall

329 effects, some hematite ore retained its original morphology (Figure 6(b)). The goethite

330 particles mostly kept the original morphology, but many cracks appeared in the matrix due to

331 the dehydration reaction at relatively low temperatures (Figure 6(c)).

332 **3.3 Sintering Conditions by Tablet Testing**

333 To better understand the sintering process, tablet experiments were conducted under various

334 temperatures with different quench methods. To determine the temperatures achieved, a

335 tablet was prepared with a type R thermocouple placed at its centre. The tablet was then

336 inserted into a furnace at 1300 °C and allowed to reach a constant temperature before it was

337 moved to the top end of furnace tube and cooled to room temperature (Figure 7). The tablet

338 temperature increased sharply when it was heated in the furnace, approaching the furnace

339 temperature within a minute. The peak heating rate was 88.5 °C/s which compares to

340 33.6 °C/s (average of the temperature rising rates from thermocouples T1 to T4 (except

341 located at the wall) for millipot experiments 1-4). The temperature of the tablet reached

342 1280 °C and 1288 °C after 1 and 1.4 minutes and plateaued at 1291 °C after 2.1 minutes. The

343 temperature change during quenching was also very fast, decreasing to below 1000 °C in

344 seconds. The peak cooling rate was 63.2 °C/s which compares to 20.9 °C/s (average of T1 to

345 T6 thermocouple rates for millipot test No. 3 in Table 1).
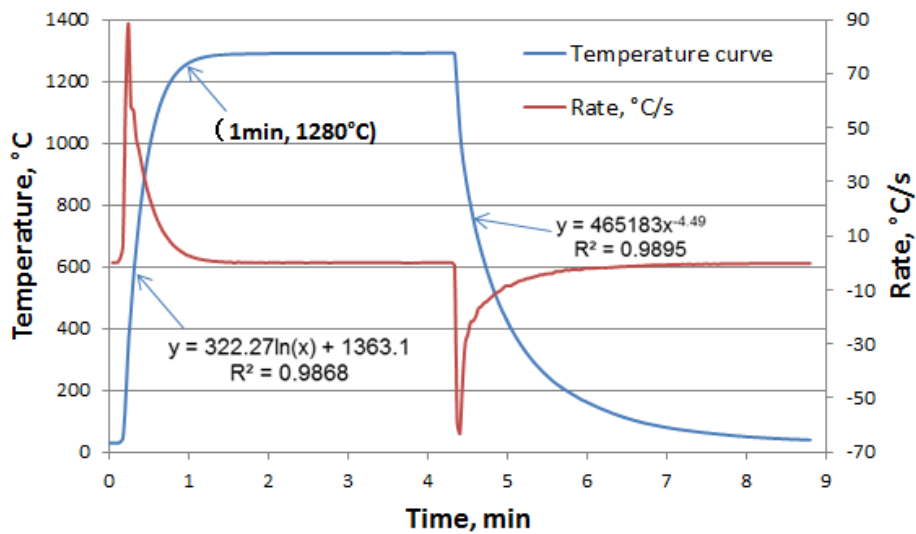
346

347 Figure 7. The temperature profile of a tablet of 6 mm in diameter heated in a furnace at

348 1300 °C and then quenched in air at room temperature.

349 Sintering at 1250 °C for 4 minutes and then quenching formed a large amount of SFCA and

350 SFCA-I (Figure 8). However, significant melting was not observed and a significant fraction

351 of primary hematite was retained. With increasing sintering temperature, pore coalescence

352 was more apparent due to increased melting as indicated by the formation of large round

353 pores. In the tablet sintering tests, the sinter blend was crushed into fine powder and then

354 pressed into tablets. Many small pores were present among the fine particles of sinter blend.

355 Along with the increase in the extent of sintering with increasing temperature, the amount of

356 sinter melt increased with improved fluidity, which helps *coalesce* the small pores into larger

19

357   pores. Especially, when a liquid phase was formed, the liquid penetrated into small pores,

358   forming denser solid/liquid phases and larger pores. The amounts of hematite, SFCA and

359   SFCA-I also decreased with increasing sintering temperature. As in Figure 8, at 1325 and

360   1350 °C, the amounts of hematite and SFCAs were minimal as hematite was not stable

361   throughout the temperature range of the tests in the atmosphere with 0.5% O_2.
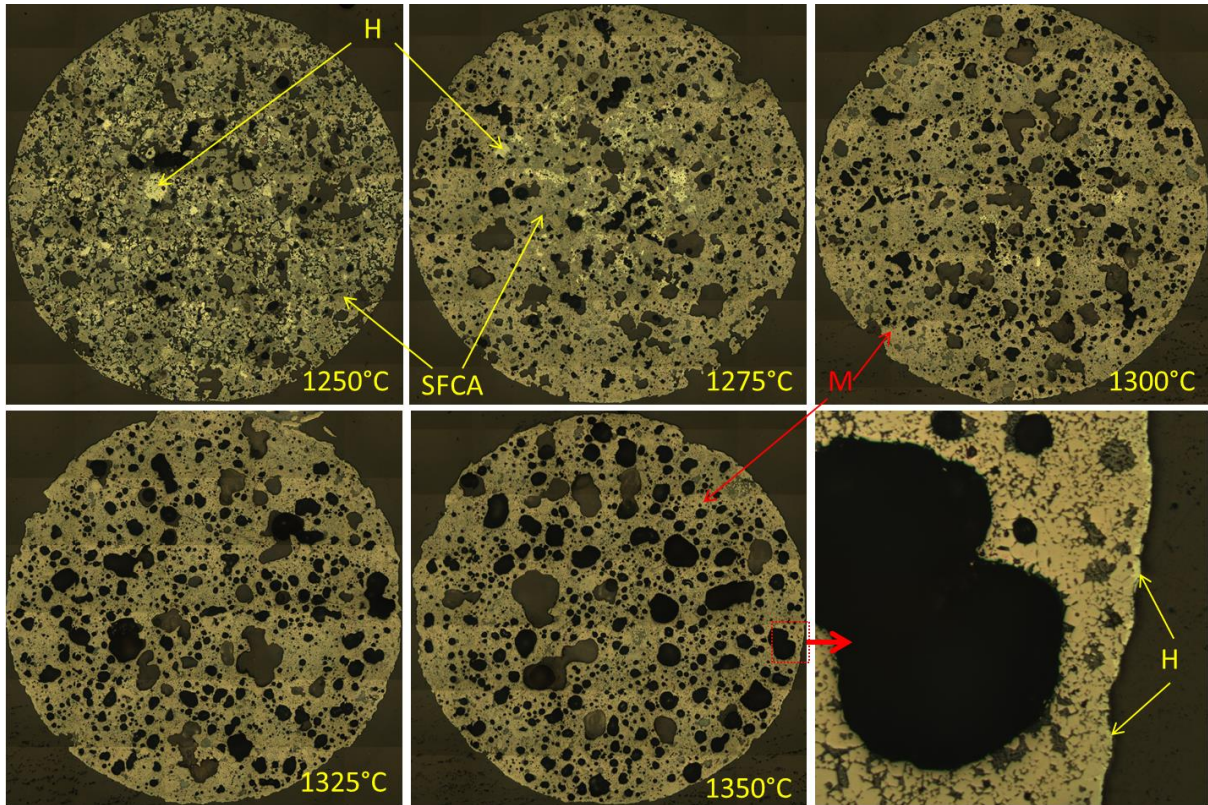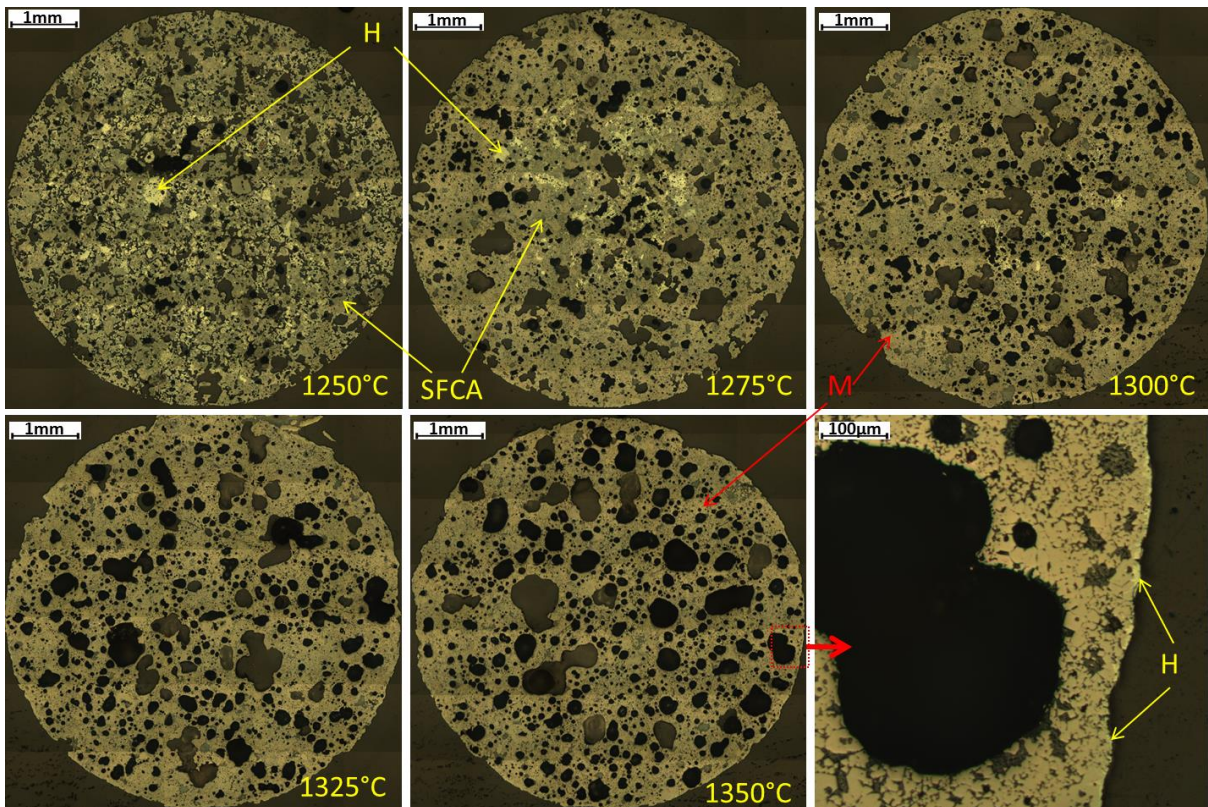
364 Figure 8. Photomicrographs of the tablets sintered at different temperatures in the 0.5% O_2

365 atmosphere for 4 minutes and then directly quenched in air to room temperature.

21

366   The decomposition of hematite to magnetite as well as oxidation of magnetite would occur at

367   different temperatures and atmospheres:

368    $6Fe_2O_3 \rightleftarrows 4Fe_3O_4 + O_2$ (1)

369   Thermodynamic calculation using FactSage shows that, in the atmosphere with 0.5% O_2, the

370   decomposition happens above 1235 °C, which implies the decomposition of hematite could

371   occur in all tablet tests of Figure 8. Under these conditions, oxygen released during hematite

372   decomposition diffused through the tablet, forming an oxygen partial pressure gradient. As a

373   result, the hematite close to the edge of the tablet decomposed faster than that at the centre.

374   This is consistent with the observation that the remaining hematite was present internally

375   within the tablets sintered at temperatures up to 1300 °C. Above this temperature, no residual

376   hematite was observed; only a very small amount of secondary hematite was observable at

377   the very surface, formed by oxidation of the magnetite during fast cooling in air.

378   From Figure 9, the addition of a 3-minute soaking stage after sintering for 4 minutes mostly

379   affected the amount of hematite in the tablets. The overall appearance of the tablets was not

380   obviously changed, although an increase of the proportion of large pores cannot be excluded.

381   At 1250 °C, three minute holding in air increased the amount of hematite throughout the

382   tablets. The increased amount of hematite was attributed to the re-oxidation of magnetite

383   during soaking in air, which was predicted by FactSage to take place below 1383 °C in air. At

384   1300 °C, additional hematite was only present at the edge of the tablet. It is also noted that

385   the small fraction of hematite present at the centre of the tablet in Figure 8 at 1300 °C

386   practically disappeared during the cooling in air (Figure 9). No obvious formation of hematite

387   was detectable in the tablets sintered at higher temperatures 1325 and 1350°C. It is speculated

388   that the lack of formation of secondary hematite was due to multiple factors, including

389   formation of molten phase and gradual replacement of the relatively reducing gas by air in

390   the furnace tube. Furthermore, the magnetite in the molten solution had a lower activity and

391   hence was more stable, while in the early stage of cooling the atmosphere was less oxidizing

392   compared with air.

393   During the soaking stage in air, oxygen diffused towards the interior of the tablets. It seems

394   that only the external layer was affected by the oxidation of magnetite at 1300 °C. The lack of

395   oxidation in the tablets sintered at temperatures above 1300 °C and then cooled in air is

396   attributed to the melting of the fine particles constituting the tablets which enclosed the

397   internal pores and suppressed the diffusion of O_2 into the tablets. The magnified image of the

398   tablet edge (Figure 9) shows that the matrix of the tablets sintered at high temperatures was

399   dense and impermeable, and hematite existed as a very thin layer at the periphery. The tablet

400   sintered at 1275°C in 0.5% O_2 atmosphere for 4 minutes followed by holding in air for 3

401   additional minutes has the most similar microstructure to the sinter products from the millipot

402   and industrial sinter plant when comparing the morphology and mineral phase composition.
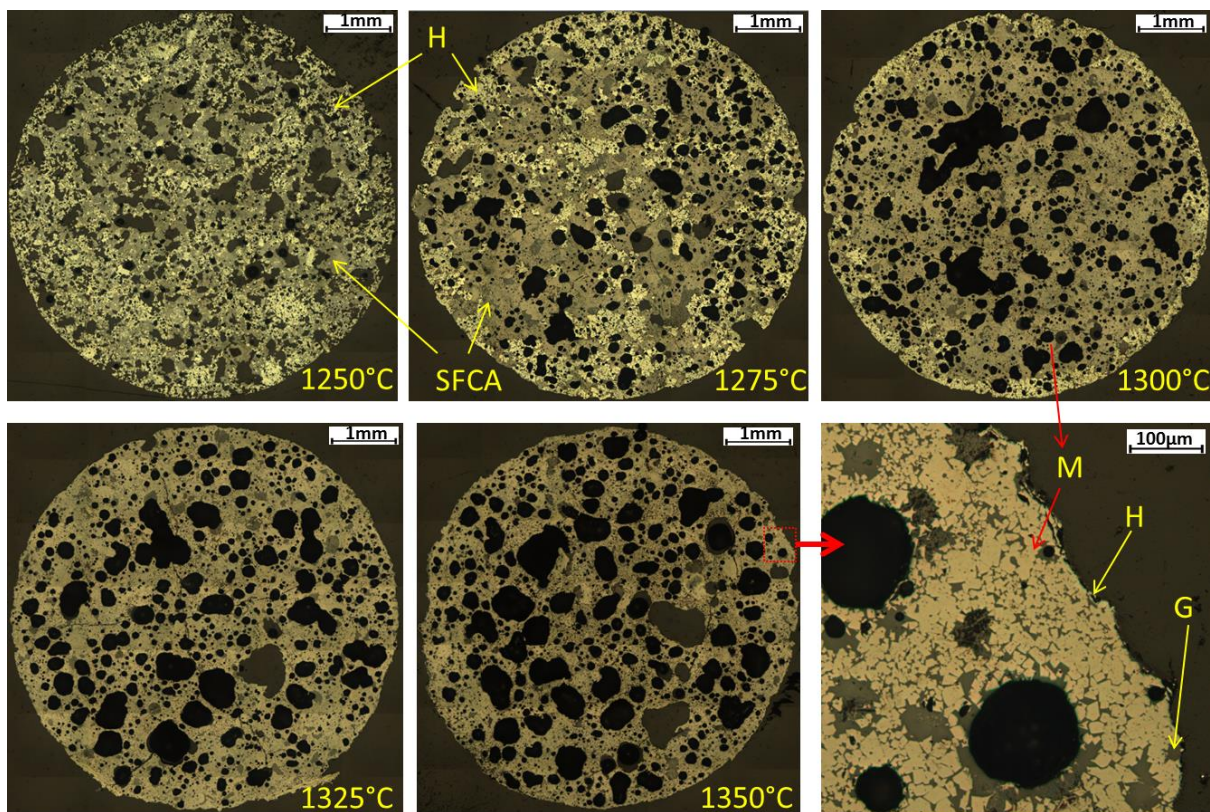
403

404   Figure 9. Photomicrographs of the tablets sintered at different temperatures in the atmosphere

405   with 0.5% O₂ for 4 minutes followed by holding in air at the lower of the sintering

406   temperature or 1250 °C for 3 minutes.

3.4 Comparison of the Mineral Compositions of Tablet, Millipot and Industrial Sinters

409   The mineral phase compositions of the sintered tablets, millipot and industrial sinter products

410   obtained by image analysis are summarized in Figure 10. The figure also includes the results

411   for industrial sinter via the point counting method. In reflectance based image analysis, glass

412   cannot be distinguished from pores, so the glass content was not quantified, and the total

413   fractions of hematite, magnetite and SFCA were normalized to 100%. Further, only the

414   combined amount of SFCA and SFCA-I was obtained, as the reflectance of these two phases

415   is essentially the same, preventing separate determination via image analysis.
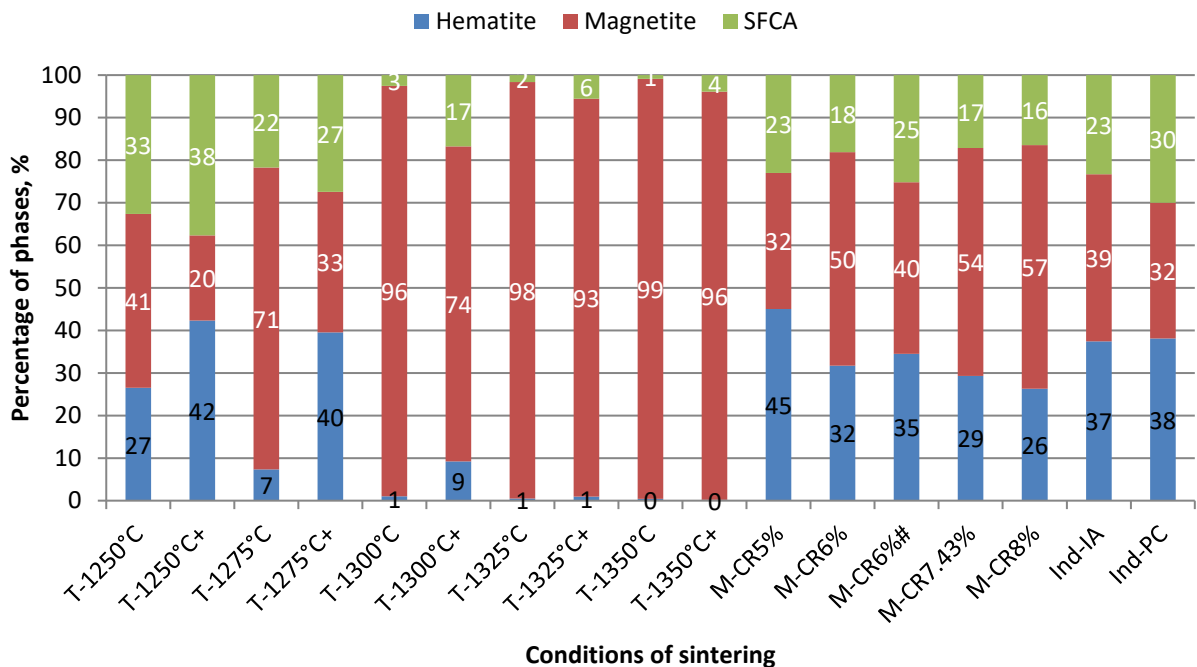
417   Figure 10. Comparison of sinter mineral phase compositions under different sintering

418   conditions (tablets, millipot and industrial). T indicates Tablet experiment at temperature and

24

419 + indicates three minutes holding in air at 1250 °C during the cooling stage; M indicates

420 Millipot run at CR (coke rate) and # indicates pressure gradient increased to 14.0 kPa/m in

421 ignition and 28.8 kPa/m in sintering process; Ind indicates Industrial sample, with IA (image

422 analysis) and PC (point counting).

423 For the industrial sinter, 37% hematite, 39% magnetite, and 23% SFCA was determined by

424 image analysis, which is the closest to the millipot sinter produced with 6% coke rate and

425 increased suction pressure (viz. 35% hematite, 40% magnetite and 25% SFCA). For the

426 millipot sinter with 6% coke rate but without the increase in suction pressure, both hematite

427 and SFCA were lower. An increase in the pressure gradient in the millipot operation caused

428 an increase in the oxygen partial pressure in the sinter bed, which made the mineral

429 composition of the sinter closer to that of industrial sinter. Increasing the coke rate above 6%

430 generated sinter products with more magnetite.

431 The sinter samples from the tablet experiments changed in mineral composition with the

432 change in sintering temperature and cooling procedure, as demonstrated by the optical

433 images. The tablets consisted of finely ground and uniformly mixed blends of iron ores and

434 fluxes, so the conditions for assimilation reactions between different constituents were more

435 favourable than in the millipot or industrial sintering process. This helps explain the

436 occurrence of sintering reactions at 1250°C or even lower temperatures when the particles

437 remained in the solid state.[1, 24] With increasing temperature, the amount of magnetite

438 increased steadily, while that of hematite and SFCA decreased. Especially at temperatures

439 above 1300°C, magnetite accounted for most of the tablets.

440 Notably, a soaking stage in air at elevated temperatures prior to final cooling improved the

441 comparability of the tablet to the mineral content in the industrial and pot sintering processes.

442 Addition of the intermediate cooling stage increased the amounts of hematite and SFCA,

443 especially at lower temperatures. Both SFCA and hematite contents reached the maxima

444 (~40%) under the "T-1250°C+" condition; at this temperature conversion of hematite to

445 magnetite is low and the high hematite content favoured the formation of SFCA, because of

446 low reduction driving force. [2, 16, 25] In the tablet sintered at 1275°C, the increased

447 temperature caused more reduction and formation of melting phase. Reoxidation and

448 recrystallisation during the intermediate soaking stage generated a similar mineral

449 composition and structure to that of industrial sinter (Figure 11).

450
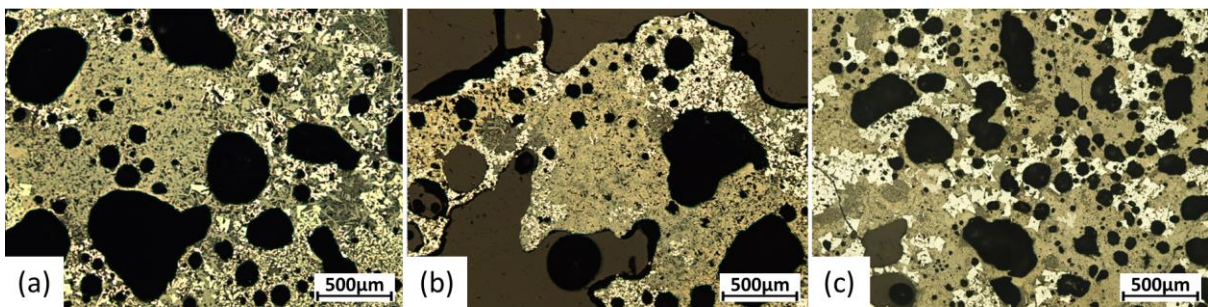
451 Figure 11. Comparison of three sintering scales: (a) industrial; (b) millipot under M-CR6%#;

452 (c) tablet under T-1275 °C+.

453 Overall, the microstructure and mineral phase composition of the industrial sinter were most

454 like the sintered tablet "T-1275°C+" and millipot sinter with industrially comparable bulk

455 density, 6% coke rate and increased suction pressure. In millipot, compaction not only

456 increases the overall bulk density, but also improves uniformity across the column diameter,

457 reducing peripheral gas flow minimizing the wall affected zone. The pressure gradient and

458 hence overall gas flowrate were increased to achieve comparable flame front speeds. With a

459 higher coke rate offsetting heat losses to the wall and increased waste gas volume to regain

460 target centreline temperatures. The similar microstructure and phase composition achieved

461 indicate that the gas atmosphere in the analyzed central portion was similar to that in the

462 industrial sinter.

463 Overall, based on the results in this study, the millipot sinter, except the near-wall product,

464 can represent industrial sinter, which bridges the gap between sintered tablets and larger scale

465 pots or full plant scale. The millipot can therefore be used as a tool for designing larger scale

466 experiments or sintering trials.

467 **4. Conclusions**

468 To determine the feasibility of small-scale pot testing, a 'millipot' facility was established to

469 examine the sintering performance of iron ores and other non-traditional ferrous materials.

470 Three sinter processing methods, viz. tablet, millipot and industrial sinter plant, were

471 evaluated and sinter products compared using the same blend. The major findings are

472 summarized as follows:

473 1) For the millipot, some experimental adjustments have to be made to achieve conditions

474   comparable to full scale sintering, including:

475   a. mechanical compaction, to increase bulk density of the sinter bed, which

476   decreases the flame front speed (FFS) and the wall effect;

477   b. coke rate increase, to offset high heat loss from the small diameter column;

478   and

479   c. suction pressure increase, to adjust the oxidizing atmosphere during sintering.

480   With these adjustments, the millipot achieved sintering conditions in a similar range to the

481   industrial process (density of sinter bed, temperature, and FFS), and a sinter product with

482   similar microstructure and mineral composition. It was not possible to fully eliminate the

483   wall effect in the small diameter millipot set-up.

484 2) Based on a comparison of microstructure and mineral composition of the sinter products

485   produced:

486   a. a tablet sintered at 1275 °C with 0.5% O_2 for 4 minutes, followed by further

487   sintering in air for 3 minutes; and

488   b. a millipot sinter produced with coke rate 6%, suction pressure 14.0 kPa/m

489   during ignition and 28.8 kPa/m during sintering

490 were most similar to the industrial sinter investigated.

Acknowledgements

REFERENCES

1. A.K. Biswas, *Principles of Blast Furnace Ironmaking.* Cootha Publishing House, 1981.
2. L. Lu, *Iron Ore: Mineralogy, Processing and Environmental Sustainability.* 2015: Elsevier.
3. J. Clout and J. Manuel, *Fundamental Investigations of Differences in Bonding Mechanisms in Iron Ore Sinter Formed from Magnetite Concentrates and Hematite Ores.* Powder Technology, 2003. **130**(1): p. 393-399.
4. Z. Wang, D. Pinson, S. Chew, H. Rogers, B. J. Monaghan, and G. Zhang, *Interaction of New Zealand Ironsand and Flux Materials.* ISIJ International, 2016. **56**(8): p. 1315-1324.
5. Z. Wang, D. Pinson, S. Chew, H. Rogers, B. J. Monaghan, and G. Zhang, *Mineral Phase Formation and Zinc Removal during Sintering of Filter Cake Wastes.* ISIJ International, 2016. **56**(4): p. 505-512.
6. L. Hsieh and J. A. Whiteman, *Sintering Conditions for Simulating the Formation of Mineral Phases in Industrial Iron Ore Sinter.* ISIJ International, 1989. **29**(1): p. 24-32.
7. Z. Wang, D. Pinson, S. Chew, H. Rogers, B. J. Monaghan, M. Pownceby, N. Webster, H. Rogers and G. Zhang, *Effects of Sintering Materials and Gas Conditions on Formation of Silico-ferrites of Calcium and Aluminium during Iron Ore Sintering.* ISIJ International, 2016. **56**(7): p. 1138-1147.
8. C. Loo and R. Dukino, *Laboratory Iron Ore Sintering Studies. 2. Quantifying Flame Front Properties.* Mineral Processing and Extractive Metallurgy, 2014. **123**(4): p. 197-203.

521 9.   H. Li, *Effect of Raw Material Composition on the Sintering Properties.* ISIJ
522   international, 2005. **45**(4): p. 551-559.
523 10. R.R. Lovel, Vining K.R., *The Influence of Fuel Reactivity on Iron Ore Sintering.* ISIJ
524   international, 2009. **49**(2): p. 195-202.
525 11. C. Kamijo, M. Matsumura, and T. Kawaguchi, *Sintering Behavior of Raw Material*
526   *Bed Placing Large Particles.* ISIJ international, 2005. **45**(4): p. 544-550.
527 12. H. Li, R. Zhou, D. J. Pinson, P. Zulli, L. Lu, R. J. Longbottom, S. J. Chew, B. J.
528   Monaghan, G. Zhang, *A Millipot Set-up for Sintering Investigation of Iron Ores.* Iron
529   Ore 2017 Conference, 2017: p. 85-90.
530 13. L. Lu, M. Adam, M. Kilburn, S. Hapugoda, *Substitution of Charcoal for Coke Breeze*
531   *in Iron Ore Sintering.* ISIJ international, 2013. **53**(9): p. 1607-1616.
532 14. K. Yajima, and S. Jung, *Data Arrangement and Consideration of Evaluation*
533   *Standard for Silico-Ferrite of Calcium and Alminum (SFCA) Phase in Sintering*
534   *Process.* ISIJ international, 2012. **52**(3): p. 535-537.
535 15. R. Chaigneau, *Complex Calcium Ferrites in the Blast Furnace Process.* Delft
536   University of Technology, 1994.
537 16. J. Jeon, S. Jung, and Y. Sasaki, *Formation of Calcium Ferrites under Controlled*
538   *Oxygen Potentials at 1273 K.* ISIJ international, 2010. **50**(8): p. 1064-1070.
539 17. N. A. Webster, M. I. Pownceby, I. C. Madsen, A. J. Studer, J. R. Manuel and J.
540   A.Kimpton, *Fundamentals of Silico-ferrite of Calcium and Aluminum (SFCA) and*
541   *SFCA-I Iron Ore Sinter Bonding Phase Formation: Effects of CaO: SiO$_2$ Ratio.*
542   Metallurgical and Materials Transactions, 2014. **45**(6): p. 2097.
543 18. M. Pownceby and J. Clout, *Importance of Fine Ore Chemical Composition and High*
544   *Temperature Phase Relations: Applications to Iron Ore Sintering and Pelletising.*
545   Mineral Processing and Extractive Metallurgy, 2003. **112**(1): p. 44-51.
546 19. M.S. de Magalhães, and P.R.G. Brandao, *Microstructures of Industrial Sinters from*
547   *Quadrilatero Ferrifero's Iron Ores, Minas Gerais State, Brazil.* Minerals
548   Engineering, 2003. **16**(11): p. 1251-1256.
549 20. N. V. Scarlett , M. I. Pownceby, I. C. Madsen and A. N. Christensen, *Reaction*
550   *Sequences in the Formation of Silico-ferrites of Calcium and Aluminum in Iron Ore*
551   *Sinter.* Metallurgical and Materials Transactions B, 2004. **35**(5): p. 929-936.
552 21. M. Sasaki and Y. Hida, *Consideration on the Properties of Sinter from the Point of*
553   *Sintering Reaction.* Iron and Steel, 1982. **68**(6): p. 563-571.
554 22. L. Hsieh and J. A. Whiteman, *Effect of Oxygen Potential on Mineral formation in*
555   *Lime-fluxed Iron Ore Sinter.* ISIJ International, 1989. **29**(8): p. 625-634.
556 23. Y. Hida, J. Okazaki, K. Itoh, M. Sasaki, *Formation Mechanism of Acicular Calcium*
557   *Ferrite of Iron Ore Sinter.* Tetsu-to-Hagane(J. Iron Steel Inst. Jpn.), 1987. **73**(15): p.
558   1893-1900.
559 24. J.H.Strassburger, *Blast Furnace Theory and Practice.* Vol. 2. 1969: Taylor & Francis.
560 25. M. Gan, X. Fan, and X. Chen, *Calcium Ferrit Generation During Iron Ore*
561   *Sintering—Crystallization Behavior and Influencing Factors*, in *Advanced Topics in*
562   *Crystallization.* 2015, InTech.
563
564

565 Figure 1. Schematics of laboratory sintering set-ups: (a) Millipot; (b) vertical electrical

566 furnace.

567 Figure 2. Optical images of industrial sinter. Q: quartz; PH: primary hematite; SH: secondary

568 hematite; M: magnetite; S: silicate; SFCA: platy shape of silico-ferrite of calcium and

569 aluminum; SFCA-I: acicular shape of silico-ferrite of calcium and aluminum.

570 Figure 3. The changes of the bed height and average bulk density with the loaded weight. The

571 bed height lines overlap.

572 Figure 4. Temperature and suction pressure profiles during millipot sintering under different

573 coke rates. (a) Coke rate = 5.0%; T2: wall temperature, and T3, T4, T6: centre temperatures;

574 (b) Coke rate = 6.0%; T2: wall temperature, and T3, T5, T6: centre temperatures; (c) Coke

575 rate = 7.4%; T1 - T6: centre temperatures; (d) Coke rate = 8.0%; T2: wall temperature, and

576 T1, T3, T4, T6: centre temperatures; (e) Coke rate = 6.0%; T2, T3: wall temperatures, and

577 T4, T6: centre temperatures; increased suction pressure. T7: flue gas temperature in all plots.

578 Figure 5. Photographs of the sinter core from testing with 6% coke rate at increased suction

579 pressures. (a) side view; (b) cross-section view.

580 Figure 6. Photomicrographs of the sinter core in Figure 5: (a) cross-section of the sinter core;

581 (b), (c) the edge of the core at different section; (d) the centre section of the core; (e), (f) the

582 rectangular areas as marked in (d). GO: goethite ore; HO: hematite ore; L: larnite.

583 Figure 7. The temperature profile of a tablet of 6 mm in diameter heated in a furnace at

584 1300 °C and then quenched in air at room temperature.

585 Figure 8. Photomicrographs of the tablets sintered at different temperatures in the atmosphere

586 with 0.5% O_2 for 4 minutes and then directly quenched in air at room temperature.

587   Figure 9. Photomicrographs of the tablets sintered at different temperatures in the atmosphere

588   with 0.5% O_2 for 4 minutes followed by holding in air at the lower of the sintering

589   temperature or 1250 °C for 3 minutes.

590   Figure 10. Comparison of sinter mineral phase compositions under different sintering

591   conditions (tablets, millipot and industrial). T indicates Tablet experiment at temperature and

592   + indicates three minutes holding in air at 1250 °C during the cooling stage; M indicates

593   Millipot run at CR (coke rate) and # indicates pressure gradient increased to 14.0 kPa/m in

594   ignition and 28.8 kPa/m in sintering process; Ind indicates Industrial sample, with IA (image

595   analysis) and PC (point counting).

596   Figure 11. Comparison of three sintering scales: (a) industrial; (b) millipot under M-CR6%#;

597   (c) tablet under T-1275 °C+.